

# On a Methodology for Robust Segmentation of Non-Ideal Iris Images

Jinyu Zuo, *Student Member, IEEE*, Natalia A. Schmid, *Member, IEEE*

Jinyu Zuo is with the Lane Department of Computer Science and Electrical Engineering, West Virginia University, Morgantown, WV 26506, USA. E-mail: jzuo@mix.wvu.edu.

Natalia A. Schmid (contact author) is with the Lane Department of Computer Science and Electrical Engineering, West Virginia University, Morgantown, WV 26506, USA. Phone: 304-293-0405x2557. E-mail: Natalia.Schmid@mail.wvu.edu.

## Abstract

Iris biometric is one of the most reliable biometrics with respect to performance. However, this reliability is a function of the ideality of the data. One of the most important steps in processing non-ideal data is reliable and precise segmentation of the iris pattern from remaining background. In this paper, a segmentation methodology that aims at compensating various nonidealities contained in iris images during segmentation is proposed. The virtue of this methodology lies in its capability to reliably segment non-ideal imagery that is simultaneously affected with such factors as specular reflection, blur, lighting variation, occlusion and off-angle images. We demonstrate the robustness of our segmentation methodology by evaluating ideal and non-ideal datasets, namely Chinese Academy of Sciences iris data version 3 Interval subdirectory (CASIA III INT), Iris Challenge Evaluation (ICE) data, West Virginia University (WVU) data, and WVU Off-angle data. Furthermore, we compare our performance to that of our implementation of Camus and Wildes's algorithm, and Libor Masek's algorithm. We demonstrate considerable improvement in segmentation performance over the former mentioned algorithms.

## Index Terms

Iris recognition, iris segmentation, texture segmentation, biometrics.

## I. INTRODUCTION

Current iris recognition algorithms that have potential for high recognition performance require highly constrained subject presentation. When this constraint is removed or unavailable, such as in surveillance applications or “iris at a distance”, the quality of the data may be degraded by heterogenous factors [1]. These factors, such as specular reflection, lighting variation, blur, off-angle, and occlusion negatively impact segmentation and recognition performance as verified by Kalka et al [2], [3] and Chen et al [4] in their works on iris image quality.

Classically, pupil and iris regions have been localized using efficient integro-differential operators as defined by Daugman [5]. This operator remains in use today for the majority of commercial systems. Wildes [6] introduced pupil and iris localization by use of edge detection which is followed by a circular Hough transform. A number of recent approaches, based on variants of the former methodology that utilize the Hough transform have been developed (for example, [7], [8], [9]). Other algorithms employ morphological operators [10] and ellipse fitting [11], [12] to cope with the non-circular shape of the pupil/iris. One limitation concerning these algorithms is that design and testing was developed for ideal data. This may result in significant degradation of performance when the algorithms are applied to non-ideal imagery.

There has been some work focusing on non-ideal iris, specifically off-angle [13], [14], or less constrained environments [15]. However, these works mostly focus on bringing off-angle iris images into frontal view in order to involve iris recognition algorithms designed for frontal view ideas irises, rather than dealing with the segmentation aspects related to this factor. Proen  a and Alexandre [1] identify a more noise tolerant feature set, consisting of pixel location and intensity, which is then used to construct an edge map followed by a circular Hough transform for localization. They demonstrate good results when evaluating the UBIRIS dataset [16]. One disadvantage with this approach is that inexact localization can result from off-angle images because of the circular fit. There are many other publications that focus on particular aspects related to nonideal iris and processing of nonideal iris images. We placed them in three broad categories: (1) unique approaches (for example, [17], [18] and [19]. The authors of the latter paper claim their optimal partitioning based algorithm is robust to poor illumination, blur, occlusion and eye glasses; (2) papers dealing with estimation of occlusions (for example, [20], [21], [22]); (3) papers that are dealing with specular reflections (for example, [20], [22]). The most recent trend in designing robust segmentation techniques is to apply nonparametric approaches such as active contours to describe the iris and pupil boundaries [23], [24]. In [24], besides active contour fitting on the boundaries and generalized coordinates, new off-angle image solution called “Fourier based trigonometry”, a statistical eyelash detection method, and a score normalization method are introduced.

In this work, we propose a methodology for automatic segmentation of iris images that sequentially compensates non-ideal factors present in poor quality iris images. This work is inspired by our previous (see [2] and [3]) and current work on iris image quality. Iris image quality is determined by a set of quality factors including motion and defocus blur, contrast, unbalanced illumination, occlusion, off-angle, and other factors. Factors are estimated for each iris image individually. A separate procedure to evaluate a specific quality metric is designed. The final result is presented both in the form of a vectors of individual quality values and in the form of a single number obtained by applying Dempster-Shafer combination criterion [25]. The fact that quality metrics can be estimated individually laid a foundation for this work.

This paper describes a sequence of procedures and steps that are intended to compensate detected nonidealities in iris images in order to successfully segment nonideal iris images. The following compensation steps are applied. Similar to many other segmentation methods we first detect and eliminate specular reflections through the application of hard thresholding and Partial Differential Equation (PDE)-based inpainting, respectively. Then we localize the pupil by invoking diverse information available in the image involving pupil location, intensity, and shape. We further propose a technique to eliminate occlusions resulting from the overlap of long eyelashes with the area of the pupil. This step ultimately

influences segmentation of the pupil area, which is performed next. Both the pupil and iris in an iris image are segmented by fitting a rotated ellipse, an ellipse parameterized by the parameters of main axes, center point, and the angle of rotation. During the iris segmentation, we apply a contrast balancing procedure to ensure correct segmentation of bright and shadowed portions of the iris. Simultaneously with iris boundary we estimate the occlusion mask by applying an edge detector and slightly smearing the mask to ensure connected edges.

The rest of this paper is organized as follows. Section II describes our segmentation methodology for a pupil and iris localization. This section also lists preprocessing steps required for successful segmentation in the presence of non-idealities. Section III illustrates the performance of our segmentation algorithm using non-ideal data such as CASIA III INT (CASIA for Institute of Automation, Chinese Academy of Sciences) [26], ICE [7], [27], WVU [28] and WVU off-angle datasets [29]. Finally, a summary and conclusions are presented in Section IV.

## II. SEGMENTATION METHODOLOGY

Traditionally, iris segmentation algorithms perform a number of steps. Ours includes: (A) preprocessing; (B) pupil segmentation; (C) iris segmentation; (D) occlusion estimation and (E) unwrapping. A general block-diagram of the steps in the proposed segmentation algorithm is shown in Fig. 1. Although some of those steps appear to be similar to steps in traditional iris segmentation algorithms, each step in Fig. 1 targets compensation of a specific nonideality and includes a procedure for compensation of the nonideality in addition to traditional processing. The sections below provide details of each step.

### A. Preprocessing

The preprocessing of iris images consists of detection of specular reflections, their removal and denoising of images.

1) *Inpainting of Specular Reflections*: Due to high intensities of specular reflections and large gradient values along their boundaries, if not successfully removed, specular reflections substantially degrade performance of an intensity- and gradient-based segmentation algorithm. The details of preprocessing are provided below.

Let  $A(n_1, n_2)$  be an image intensity at a location  $(n_1, n_2)$ . In our approach specular reflections are localized through application of a thresholding function,  $\gamma(n_1, n_2)$ . An intensity value of a pixel  $(n_1, n_2)$  is considered as a specular reflection if the intensity value  $A(n_1, n_2) \geq \gamma(n_1, n_2)$ . For specular reflections within the area of the pupil, a threshold of value  $\gamma_1$  is used. The value of this threshold influences the

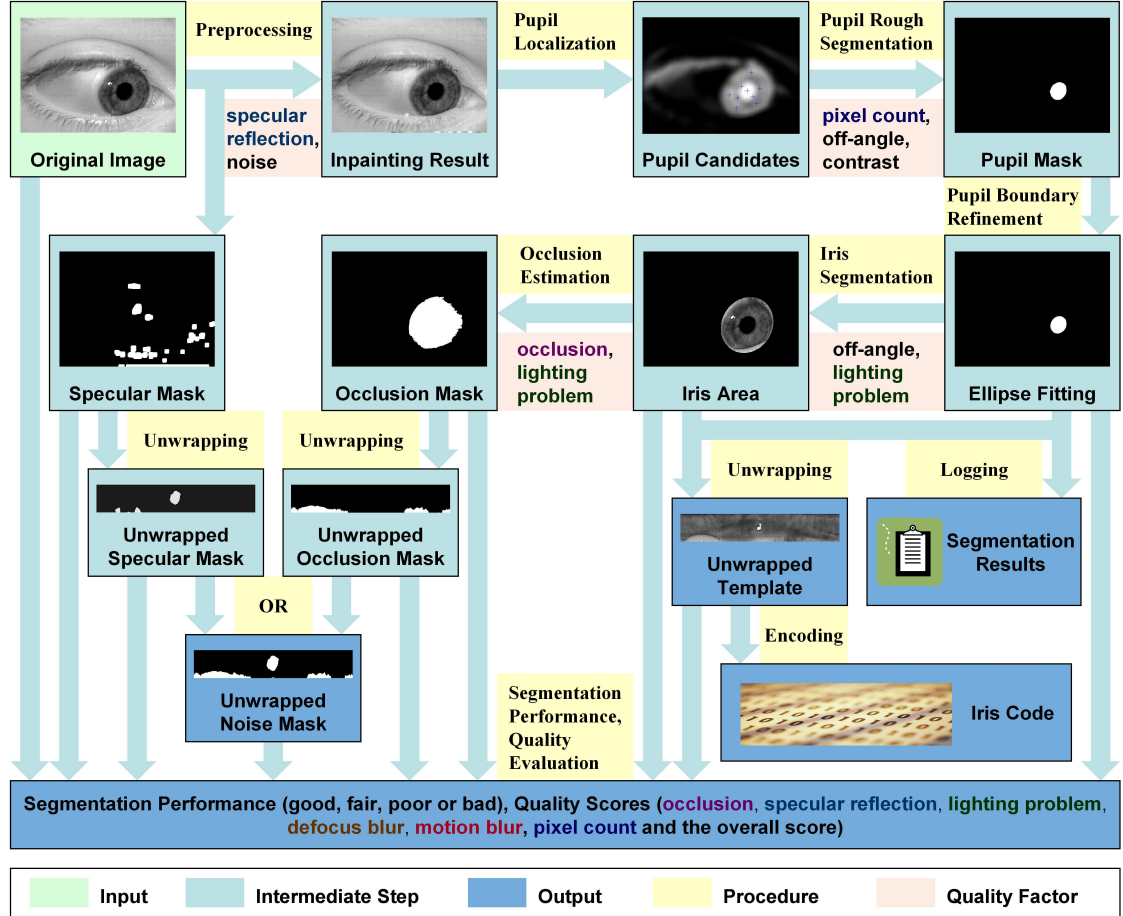


Fig. 1. Block diagram of the iris segmentation procedure.

result of inpainting, which is important for the intensity-based pupil area selection described in the following subsection. For specular reflections inside of the iris area, a threshold  $\gamma_2 > \gamma_1$  is used to avoid attributing well illuminated iris areas to specular reflections. To identify a potential pupil area we introduce another threshold  $\tau$ . In our implementation,  $\gamma_1$  and  $\tau$  are assigned the same value. Therefore, the final thresholding function  $\gamma(n_1, n_2)$  is described as:

$$\gamma(n_1, n_2) = \begin{cases} \gamma_1, & \text{pixel } (n_1, n_2) \text{ is located inside of the potential pupil area determined by } \tau, \\ \gamma_2, & \text{otherwise,} \end{cases} \quad (1)$$

where parameters  $\gamma_1$ ,  $\gamma_2$  and the maximum pupil intensity value  $\tau$  have to be preset. These parameters depend on the type of the sensor used to acquire images and the environment. The procedure results in a rough masking of the regions of specular reflections. Localized specular reflections are further refined

based on the shape and connectivity properties of masked areas. Although a set of tuned parameters used to process data to demonstrate performance of the proposed segmentation algorithm in Sec. III is suitable for a number of iris capture devices operating in near-IR range, our specular reflection detector has to be recalibrated, that is,  $\gamma_1$ ,  $\gamma_2$ ,  $\tau$  have to be evaluated, if new capture devices or new environmental set ups are used. The parameters can be easily estimated from a small set of sample iris images when capture device or environmental setup change.

Once specular reflections are detected, they have to be treated individually based on their location in the image. A special care has to be taken of the specular reflections located inside the pupil. For this purpose, the specular reflections located inside of the possible pupil regions are inpainted first. To compensate for the missing data, a sparse partial differential equation (PDE)-based inpainting procedure [30] is applied to refined localized specular reflections. After inpainting, additional intensity adjustment needs to be integrated to ensure that the inpainted areas have similar intensity values as unaffected pupil areas. To adjust the intensity value, possible unaffected pupil regions have to be detected. It is assumed that they are close to the specular reflections but have a relatively low average intensity value. Once the unaffected pupil regions are detected, 0.1 quantile and 0.5 quantile intensity values of various unaffected pupil regions are used to upper and lower bound the intensity values of inpainted regions.

The complete inpainting procedure includes the following steps:

- A potential pupil area,  $mask_{p1}$ , is identified using the maximum value of pupil intensity,  $\tau$ , as a threshold. An enlarged mask  $mask_{p2}$  is obtained after closing unfilled regions.
- Potential regions containing specular reflections,  $mask_s$ , are selected using the thresholding procedure (1). The regions are further refined using relationship between neighboring points. Specular reflection areas are selected using a threshold  $\gamma$ .
- The  $mask_s$  is dilated to include all possible affected regions.
- The intersection of  $mask_{p2}$  and  $mask_s$  is selected to be inpainted region inside of the pupil denoted as  $mask_{p3}$ .
- The area  $mask_{p3}$  is inpainted, and the intensity values in the region are adjusted using the intensity information of the region  $mask_{p1} \cap mask_s$ , the intersection of  $mask_{p1}$  and  $mask_s$ .
- The region of potential specular reflections,  $mask_{s1}$ , is updated by applying the thresholding procedure (1) to the inpainted image. The resulting mask is again refined using the relationship between neighboring points.
- The  $mask_{s1}$  is expanded to include all possible affected regions.
- The region selected by  $mask_{s1}$  is inpainted.

An example of the inpainting process is shown in Fig. 2. The purpose of inpainting is not to make the

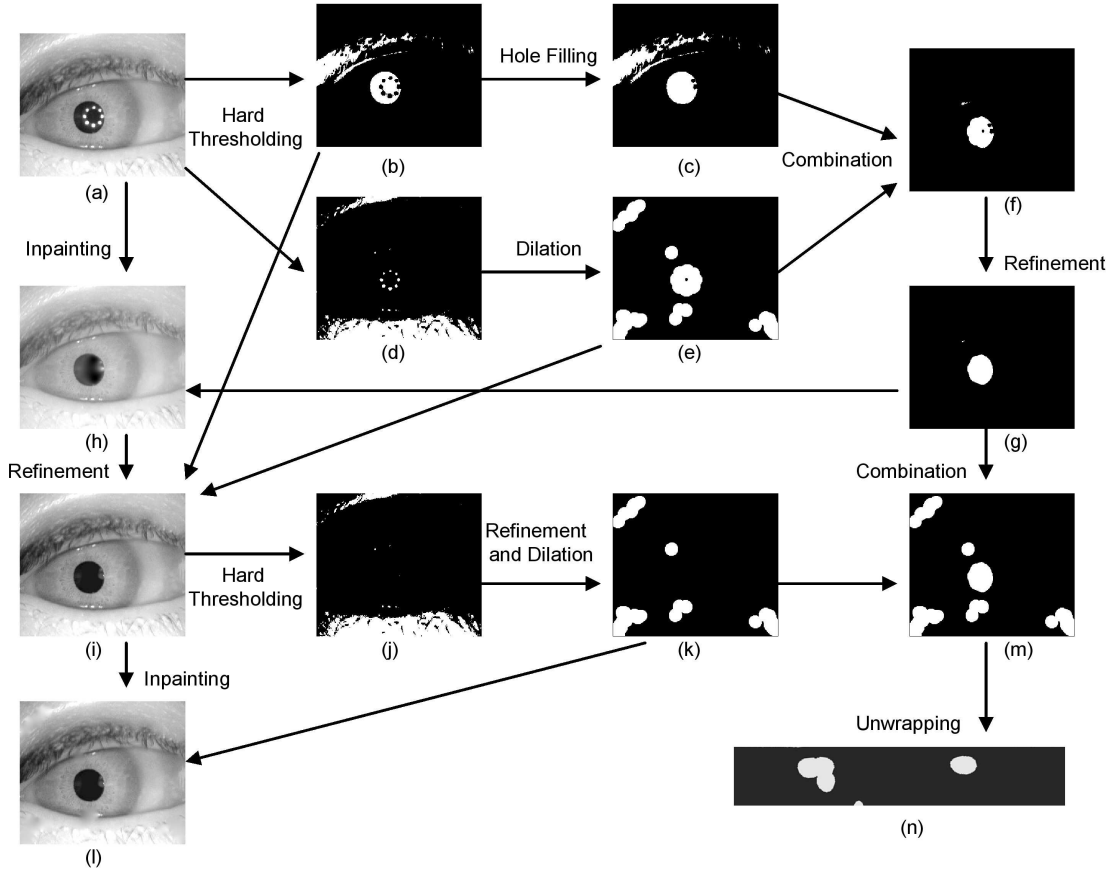


Fig. 2. Inpainting steps: (a) the original image, (b)  $mask_{p1}$  of the potential pupil area, (c) gaps in  $mask_{p1}$  are filled to obtain the mask  $mask_{p2}$ , (d) rough specular reflection  $mask_s$  is obtained using the threshold  $\gamma$ , (e) expanded specular reflection  $mask_s$ , (f) combination of (c) and (e), (g) the intersection  $mask_{p2} \cap mask_s$  of two masks, (h) result of initial inpainting, (i) refined inpainting result after intensity adjustment, (j) rough specular reflection  $mask_{s1}$  obtained using the threshold  $\gamma$  applied to (i), (k) refined and expanded specular reflection  $mask_{s1}$ , (l) final result of inpainting, (m) final specular reflection mask used to generate the template mask, (n) template mask.

image more pleasing, or to recover damaged information; it is intended to simplify the pupil segmentation procedure and increase a success rate of segmentation.

An additional factor that can be detected and removed during the initial stage of preprocessing is the additive noise. Its influence on the iris boundary detection and estimation of occlusions is due to high absolute gradient values present in noisy images.

2) *Denoising*: To eliminate the effect of noise we choose to work with a two-dimensional adaptive Wiener filter. The values of the mean,  $\mu$ , and variance,  $\sigma^2$ , are estimated locally first for each pixel

$(n_1, n_2)$  in the original image  $A$ :

$$\mu = \frac{1}{NM} \sum_{n_1, n_2 \in \eta} A(n_1, n_2),$$

$$\sigma^2 = \frac{1}{NM} \sum_{n_1, n_2 \in \eta} A^2(n_1, n_2) - \mu^2,$$

where  $\eta$  is the  $N$ -by- $M$  local neighborhood of each pixel in the image  $A$ . In our current implementation  $N$  and  $M$  are set to 5. Then the denoised image  $B$  is given by:

$$B(n_1, n_2) = \mu + \frac{\sigma^2 - v^2}{\sigma^2} (A(n_1, n_2) - \mu).$$

where  $v^2$  is the average of all locally estimated variances.

The result of noise removal is especially noticeable in low resolution images (for instance, images from CASIA I dataset). The noise removal often improves quality of unwrapped images.

After the preprocessing step is complete, the image is submitted for segmentation.

### B. Pupil Segmentation

The pupil segmentation is composed of a number of steps. This includes (1) contrast stretching, a step that ensures clarity of the boundary between the pupil and iris; (2) smoothing step that removes extreme values without reducing sharpness of the image; (3) pupil localization that finds a potential location of the pupil; (4) rough segmentation of the pupil; (5) refinement of a roughly segmented pupil; (6) ellipse fitting into the pupil boundary; and (7) evaluation of precision of pupil segmentation. The rest of the section provides details of the steps above.

1) *Contrast Enhancement (Normalization):* Iris images acquired under nonideal experimental set up often have low contrast, especially along the boundary between pupil-iris and iris-sclera. To enhance the contrast we implement the following procedure:

$$B(n_1, n_2) = \min \left( 255, \frac{255 (A(n_1, n_2) - \min(A))}{\max(128, q_{0.4}(A)) - \min(A)} \right),$$

where  $A$  is the image before the contrast enhancement,  $B$  is the image after the contrast enhancement,  $\min()$  is the function that returns the minimum value,  $\max()$  is the function that returns the maximum value, and  $q_x()$  is the function that returns the  $x$  quantile of image intensities [31].

Contrast enhancement is a necessary procedure that ensures the correct pupil segmentation. The noise and the other strong disturbances caused by the near pupil sphincter muscle and eyelashes are eliminated by performing a smoothing step described below.

2) *Smoothing*: To smooth the enhanced image we apply a median filter [32]. The value of an output pixel is determined by the median of the pixels in the neighborhood, rather than the mean. The median is much less sensitive to outliers compared to the mean. Median filtering removes these outliers without reducing the sharpness of the image. The size of the median filter depends on the resolution of the image to be smoothed. As the pupil segmentation procedure is intensity and gradient based, the smoothing of the image is important for the images with low contrast or with noisy pupil area. It also helps the detection of limbic boundary, since a large window median filter can remove misleading edges that can be observed inside of the iris area. This step may not be useful for good quality images, but does not alter performance in this case.

3) *Pupil Localization*: After image is enhanced and denoised, it is further subjected to pupil localization procedure. Two assumptions are made that are required to hold under both ideal and non-ideal settings:

- The pupil area has the smallest intensity values in the image. Note that this assumption can be reversed in order to address the “red eye effect.”
- The shape of the pupil can be described relatively well by a circle or ellipse.

The first assumption is valid under condition that the amount of the light reflected back from the pupil is relatively small. The light is typically reflected from the cornea’s convex surface. This is valid under the ideal setting. The second assumption is valid both under ideal and non-ideal settings.

To locate the pupil we use two steps: (1) pupil candidates are selected based on the circular shape and (2) the best pupil candidate is selected based on intensity information and location with respect to the image center.

Potential candidates are selected by applying a circular Hough transform. When evaluating non-ideal data, eyelashes and strong specular reflections can introduce “fake” pupil candidates. A number of candidates can be removed by introducing a smoothing step prior to applying the Hough transformation.

After candidates have been selected, intensity and location information is used to find the optimal candidate. An adjusted intensity value for each candidate is generated based on another justifiable but relatively weak assumption: the pupil is normally located near the center of the iris images. The adjusted intensity value  $w_i$  of a candidate  $i$  is calculated based on convolved intensity value and its distance from the image center. Mathematically this is described as follows:

$$w_i = \frac{I'_i}{1 + 3d_i^2},$$

where  $d_i$  is the distance between the candidate and the image center, and

$$I' = (255 - I) * \mathbf{1}_{n \times n},$$

is the result of the convolution of the inverted image  $255 - I$  with a square matrix of all ones of size  $n \times n$ . The value of  $n$  is selected based on the size of the image.  $I'_i$  is the intensity value of a candidate at the location  $i$ . The candidate with the largest adjusted intensity is selected as the optimal candidate. Fig. 3 is an illustration of this process. Once the optimal candidate is selected, the pupil can be roughly

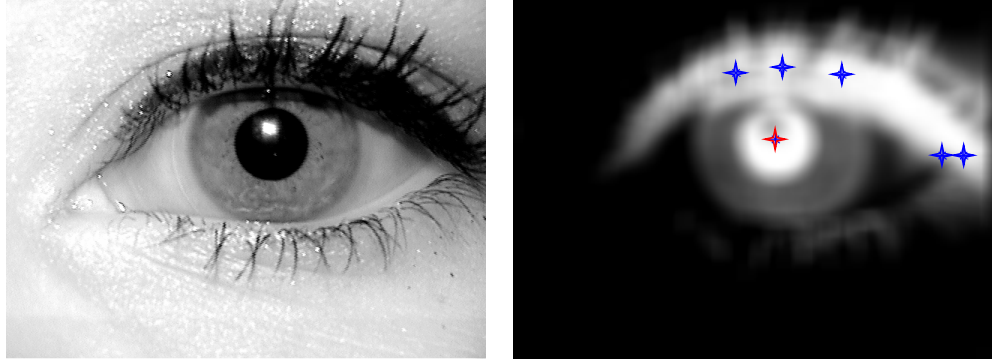


Fig. 3. In this example, six pupil candidates are selected based on a circular shape of bright regions. Then the intensity information is used to select the optimal candidate with the largest intensity value.

segmented using similarity of the intensity values.

In some cases, the assumptions stated earlier may not hold. The method described above will help to consistently select the true pupil candidate. When the true pupil candidate is located near the boundary, the candidate can be correctly selected if no other pupil like area exists (with low intensity and circular shape) within the image. In this case the true candidate will return the highest adjusted value  $w_i$  in spite of a higher value of penalty  $d_i$ . The assumption that the shape of the pupil can be described relatively well by a circle or ellipse, may not hold true for heavily occluded iris images or images with strong off-angle. Again, the true pupil candidate can be correctly selected if no other pupil like area exists (with low intensity and circular shape). Circular Hough transform is tolerant to partial occlusions or imperfect circular boundaries. In this case the true pupil area will be among candidates for pupil center and will return the highest adjusted value  $w_i$  due to the lowest average intensity of the surrounding area.

4) *Rough Segmentation of the Pupil:* A  $5 \times 5$  neighborhood around the optimal candidate is used to identify the initial minimum and maximum intensities used for searching the pupil area. This intensity range is refined based on the rough estimation of the pupil shape and the gradient information along the region boundary. The pupil area is assumed to be relatively well described by a circular shape and have a clear boundary. We further present a summary of the evaluation criteria:

- The size of the selected area should be larger than a threshold. In our experiments, we use 100.

- The average gradient value along the boundary has to be evaluated. The true pupil boundary returns the maximum gradient value.
- The difference between the original shape and the ellipse fitted into the area have to be less than a threshold, we use 13%. This threshold may need tuning for some databases to achieve the best performance.

After the rough evaluation of the pupil boundary we perform a few processing steps to compensate for eyelash occlusion and specular reflections on the pupillary boundary.

5) *Refinement of the Pupil Boundary*: Eyelashes can introduce “spike” like shapes along the boundary region. These “spike” like regions can be removed by analyzing the boundary locally. Fig. 4 is an illustration of this procedure. The center of mass for the rough segmentation region is used as an approximation to the pupil center. Then the boundary is scanned to find possible “spikes”. There are two kind of “spikes”; we call them “valley” type and “longhorn” type. The first type can be detected using the distance from the boundary points to the center. A valley is detected whenever the distance as a function of the orientation angle achieves a local minimum. The second type of “spikes” can be detected using angular information. Whenever the angle is decreasing first, then increasing and then decreasing again, the spike observed in this case is of “longhorn” type. Detected “spikes” are removed by using a large circle of radius equal to the twice the distance from the cutting point to the center. An example of

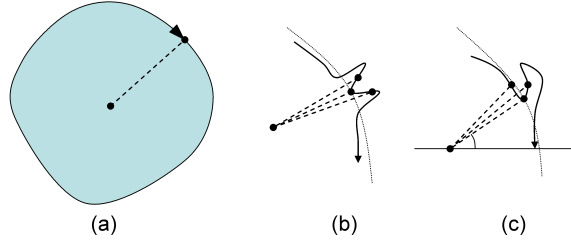


Fig. 4. “Spike” removal: (a) scanning the boundary, (b) “valley” type “spike”, (c) “longhorn” type “spike”. Dotted curves in (b) and (c) are the boundaries of the circles that are used to remove “spikes.”

“spike” removal is provided in Fig. 5. Note while the iris image in Fig. 5 is of relatively high quality in terms of iris texture, the iris area is heavily occluded by eyelashes that cause problems for an intensity based pupil segmentation.

In the case when dark long eyelashes cross the pupil area, the estimation of pupil center and the following boundary refinement will be incorrect. To remove the unwanted eyelashes, we manipulate the mask implementing dilation and erosion. The erosion breaks thin connections but it also affects



Fig. 5. “Spike” removal: (a) the original image, (b) the estimated pupil boundary, (c) removing the “spike”, (d) the refined boundary after the “spike” removal.

other regions of the pupil. To compensate for the erosion, we dilate the area around the estimated pupil location. The dilated pupil mask is combined with the original mask to keep the original boundary instead of smoothed new boundary. The procedure is illustrated in Fig. 6.

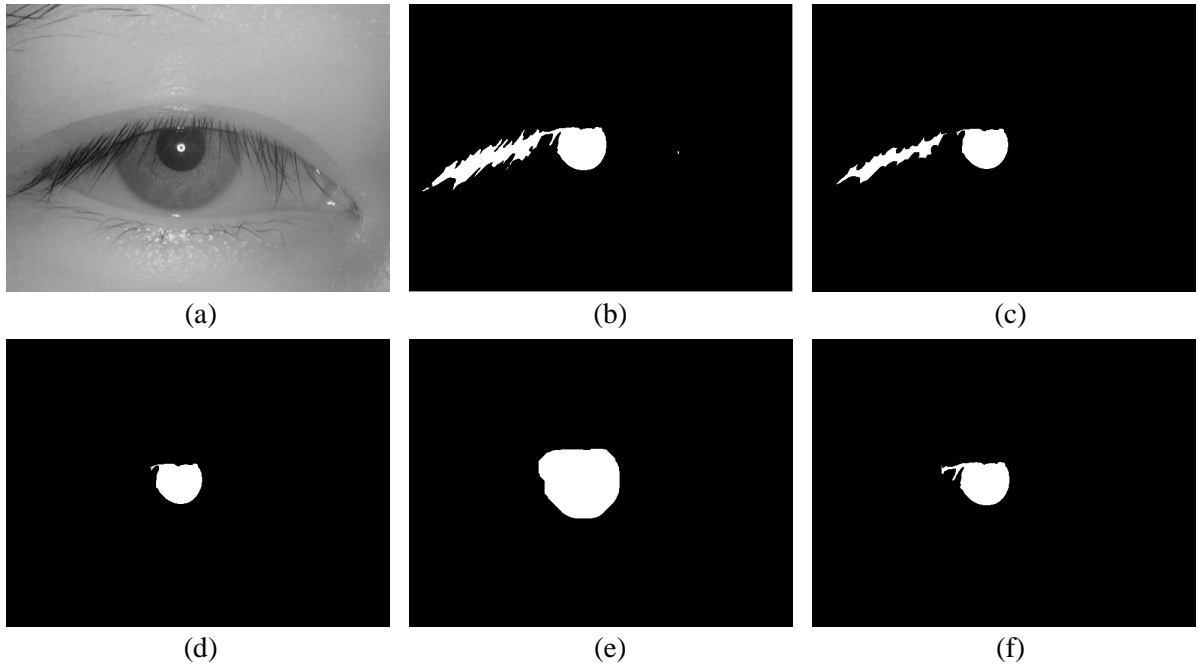


Fig. 6. Breaking unwanted connections: (a) the original image, (b) the connected mask, (c) the erosion result, (d) select the pupil region from the eroded result using the location information of the optimal candidate, (e) the dilated pupil region, (f) the result of intersecting (a) and (e).

Strong specular reflections along the pupil boundary or light colored eyelashes may cause the rough pupil boundary to become concave. We calculate the convex hull with respect to the pupil boundary in order to reduce this problem. An illustration of this process is provided in Fig. 7. As the pupil boundary affected by the specular reflections does not contain reliable information about the boundary, the following ellipse fitting procedure uses only unaffected pupil boundary. Unaffected pupil boundary can be easily

selected using a mask of specular reflections formed during the preprocessing stage.

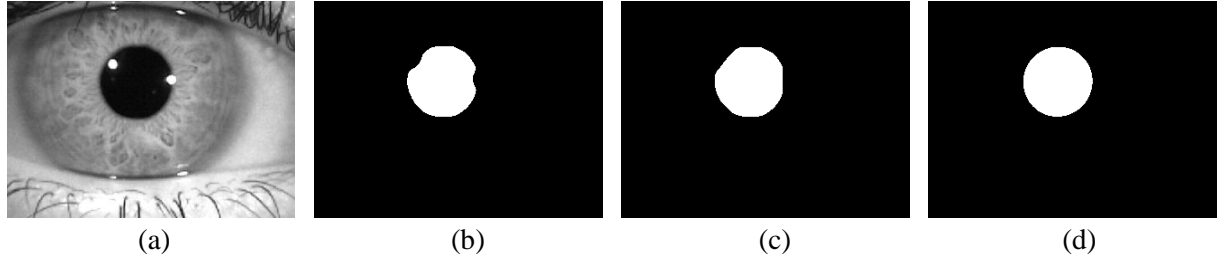


Fig. 7. Concavity removal: (a) the original image, (b) the initial concave pupil mask, (c) the convex hull result, (d) the result of ellipse fitting procedure using only unaffected pupil boundary

6) *Ellipse Fitting*: Once the boundary (or partial boundary) is determined, we apply a contour fitting procedure. There are several possible methods that can be used to accomplish the goal [5] [33],[6],[23],[34]. A graphical description of few available methods is provided in Fig. 8.

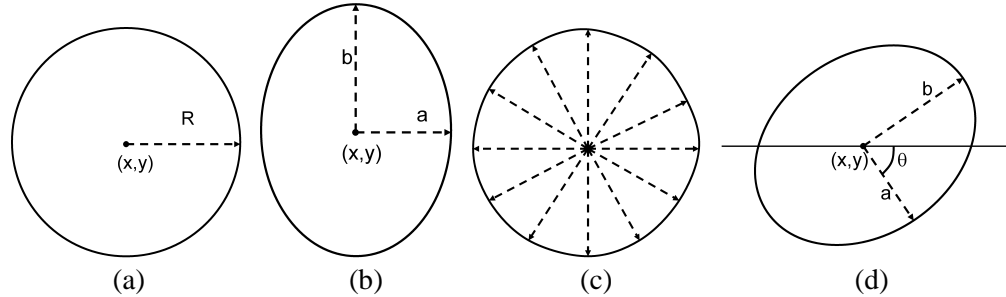


Fig. 8. Curve fitting: (a) the circle model, (b) the unrotated ellipse model, (c) the control point based model, (d) the rotated and translated ellipse model.

Classical iris segmentation techniques, such as Daugman's original segmentation algorithm [5],[33], assume a circular model for the pupil. That model has the advantage of being simple: only three parameters need to be estimated. The method provides relatively good results when applied to frontal view images. However, circular models do not describe the pupil boundary well if the iris is off-angle. In this case a more complex model is needed. For instance, an ellipse [6] can be used in place of the circle. This results in an additional parameter to evaluate. More complex models, such as b-spline-based or other nonparametric models [23] can be used to describe the boundary between the pupil and the iris. Those models, however, are sensitive to noise and occlusion if contour evolution is not well controlled. Therefore correct b-spline-based shape can not be estimated using a partial boundary. Models based on rotated and translated ellipse work well both for frontal and non-frontal iris and require only five parameters to

estimate. Mathematically a rotated ellipse is described as:

$$\frac{((x - x_{p0}) \cos \phi + (y - y_{p0}) \sin \phi)^2}{a^2} + \frac{(-(x - x_{p0}) \sin \phi + (y - y_{p0}) \cos \phi)^2}{b^2} = 1, \quad (2)$$

where  $(x_{p0}, y_{p0})$  is the center of the pupil and  $\phi$  is the angle of rotation. If the pupil boundary is distorted by specular reflections, then a partial boundary is selected using only those points which lie outside the specular reflection mask generated during the inpainting procedure. Because of occlusions caused by the eyelids, top or/and bottom parts of boundary should be avoided. The summary of the conditions for selection of the partial boundary are as follows:

- The part should not be located inside of specular reflection mask.
- The part should have a clear edge (high gradient value).
- It should be continuous (not crossed by eyelashes).
- It should be verified that the edge is a pupil edge and not an occlusion related edge.

7) *Evaluation of the Pupil Segmentation:* The goodness of the pupil boundary estimation is verified using two criteria:

- The error between the refined pupil mask and the ellipse fitted into the boundary should be small.
- If only a small part of the pupil remains unoccluded, sections of the pupil boundary have to be well separated.

If the evaluation returns a low score value, then the algorithm uses a blind circle fitting procedure. The initial pupil segmentation result is used to limit the search space by providing an approximate center of the pupil and approximate radius of the circle. This approach works well on frontal view iris images with heavily distorted pupil area.

### C. Iris Segmentation

We assume that the shapes of the iris and the pupil are similar and apply the equation (2) to segment the iris region. Other assumptions that reduce computational cost can be made. They include the assumption of the same angle  $\phi$  and the same ratio of the ellipse parameters  $a$  and  $b$ . These assumptions are especially useful when the iris is heavily occluded or it is strongly rotated.

1) *Image Translation and Inpainting:* To ensure that the search of the limbic boundary is performed over a broad range of parameters describing the ellipse, the image of an iris is translated such that the center of the pupil is aligned with the center of the image. The blank area formed due to the image

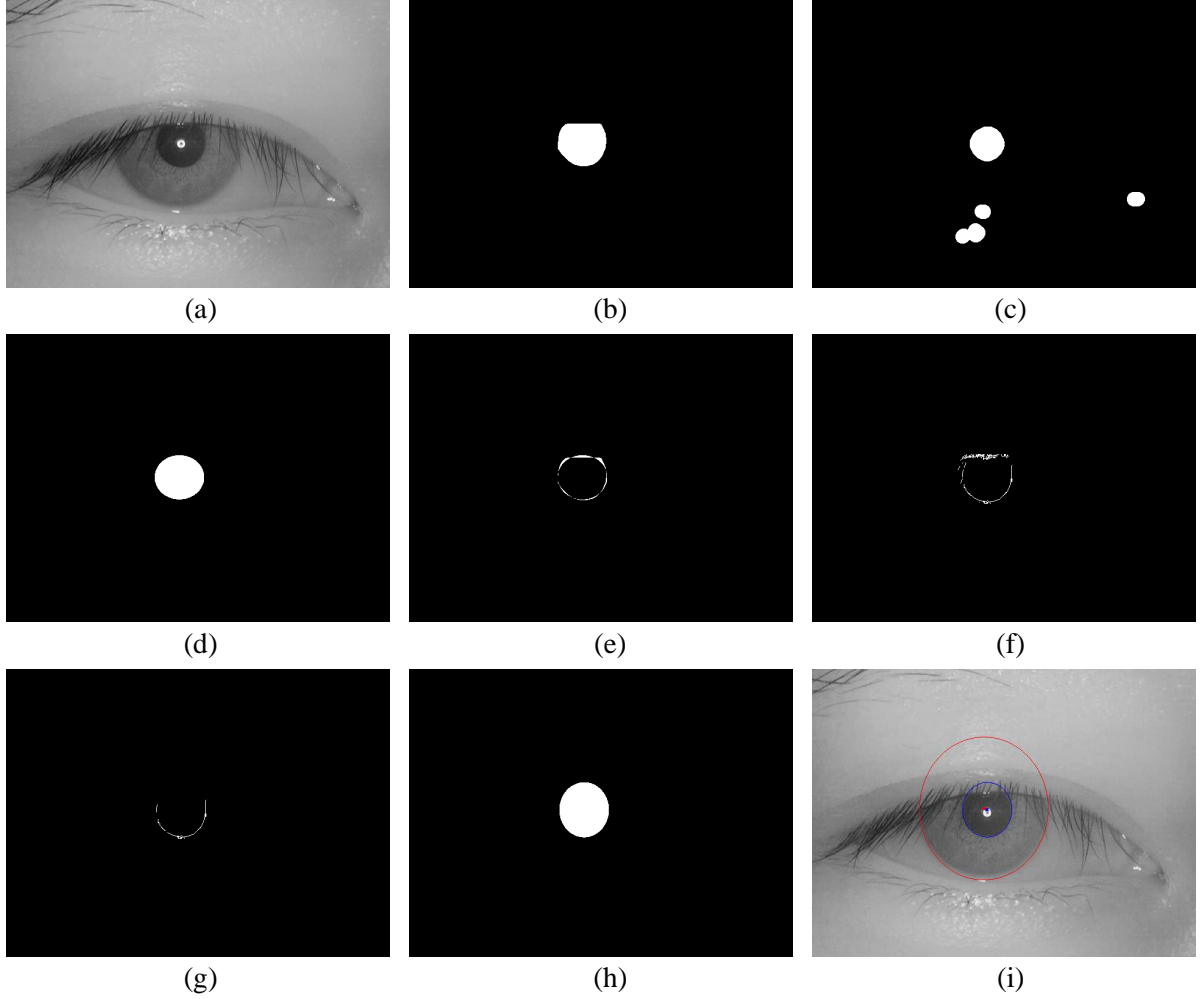


Fig. 9. Ellipse fitting: (a) the original image, (b) refined pupil mask, (c) specular reflection mask, (d) ellipse fitting result taking into account specular reflections, (e) the XOR between ellipse fitting with the original refined pupil mask, (f) the edges detected near the refined pupil boundary, (g) selected partial boundary using 4 conditions listed above, (h) the new ellipse fitting result using selected partial boundary, (i) the final segmentation result.

shift is inpanted to avoid introduction of new edges. An example of an image containing a partial iris is shown in Fig. 10.

2) *Directional Edge Detector*: We use a method similar to the Daugman's edge detector based on integro-differential operator [5]. Define a space of rotated ellipses as:

$$\left\{ (r, \phi, x_{i0}, y_{i0}) : \frac{((x - x_{i0}) \cos \phi + (y - y_{i0}) \sin \phi)^2}{(ar)^2} + \frac{(-(x - x_{i0}) \sin \phi + (y - y_{i0}) \cos \phi)^2}{(br)^2} = 1 \right\}, \quad (3)$$

where the center of the iris  $(x_{i0}, y_{i0})$  is limited to the neighborhood of the center of the pupil  $(x_{p0}, y_{p0})$ ,  $a$  and  $b$  are the parameters of the ellipse fitted into the pupil, the scale factor  $r$  is limited to be in the

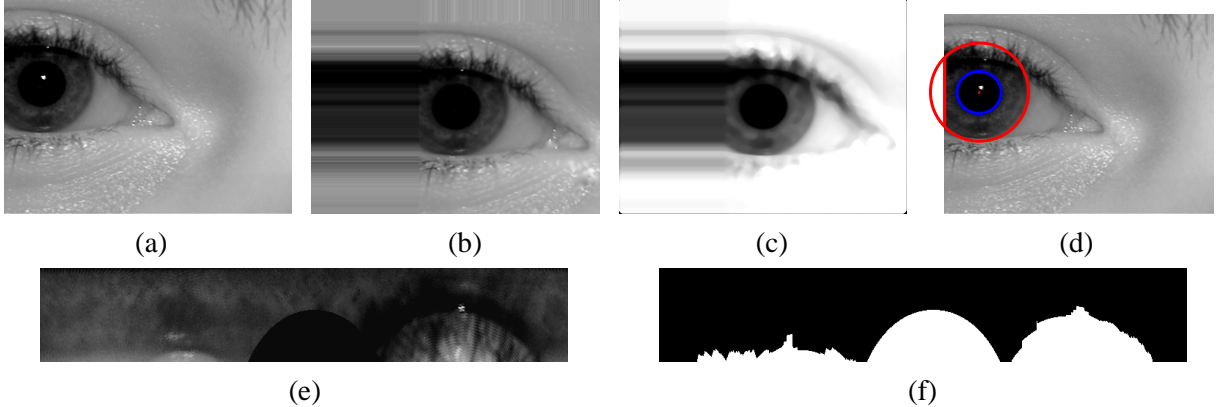


Fig. 10. Image translation procedure: (a) the original image, (b) new image after translation and impainting, (c) enhanced image, (d) segmented iris, (e) unwrapped template, (f) unwrapped template mask.

range  $[1.2, 3.5]$ , and the parameter  $\phi$  is set to be the angle of rotation of the pupil.

Then the problem of finding the rotated ellipse providing the best fit is reduced to the following optimization problem:

$$\max_{r, (x_{i0}, y_{i0})} \left[ \frac{1}{L(r, x_{i0}, y_{i0})} \oint_{B(r, x_{i0}, y_{i0})} F(\nabla(I(x, y))) ds \right], \quad (4)$$

where  $B(r, x_{i0}, y_{i0})$  is the partial boundary of the ellipse (3),  $L(r, x_{i0}, y_{i0})$  is the length of  $B(r, x_{i0}, y_{i0})$ , and  $F(\nabla(I(x, y)))$  is a function of the image gradient  $\nabla(I(x, y))$  detailed below. The function  $L(r, x_{i0}, y_{i0})$  is the normalization given by:

$$L(r, x_{i0}, y_{i0}) = \oint_{B(r, x_{i0}, y_{i0})} 1 ds.$$

Function  $F(\nabla(I(x, y)))$  returns adjusted gradient values in the normal direction to the iris boundary between the sclera and the iris region. Use of this function results in reduction of many spurious edges introduced by eyelids, eyelashes, and iris patterns while at the same time retaining those edges caused by the true iris boundary.

The function  $F(\nabla(I(x, y)))$  can be evaluated on an unwrapped image as shown in Fig. ???. The transformation of an elliptical coordinate system into a circular system is:

$$\begin{cases} (x - x_{i0}) \cos \phi + (y - y_{i0}) \sin \phi = ar \cos \theta' \\ -(x - x_{i0}) \sin \phi + (y - y_{i0}) \cos \phi = br \sin \theta', \end{cases} \quad (5)$$

where  $\theta' = (\theta - \phi')$  and  $\phi' = \arctan(\frac{a}{b} \tan \phi)$ . The angle  $\phi'$  is used to map the three o'clock point on the ellipse in the three o'clock point on the circle assuming  $\theta = 0$ . Fig. 11 is an illustration of this procedure.

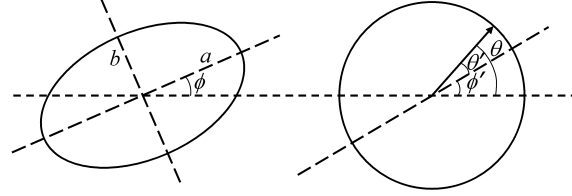


Fig. 11. A rotated ellipse (left) and its representation in a circular coordinate system.

Then the normal direction to the ellipse described by equation (3) will approximately correspond to the vertical direction in the unwrapped image denoted as  $U$ . The function  $F(\nabla(I(x, y)))$  is then evaluated on the unwrapped image  $U$  displayed in the polar coordinate system  $(r, \theta)$ :

$$F([U_\theta, U_r]) = \begin{cases} U_r & U_r > 0, |U_r| \gg |U_\theta|, \\ 0 & \text{elsewhere,} \end{cases} \quad (6)$$

where  $U_\theta$  and  $U_r$  are the gradients of image  $U$  in  $\theta$  and  $r$  directions, respectively.

The polar representation of the iris is further used to efficiently find the boundary of the iris  $B(r, x_{i0}, y_{i0})$ . We do not search for a complete boundary that excludes eyelids, eyelashes and other occlusions. We are interested in finding the regions of the iris containing the boundary between iris and sclera only. Once detected, this boundary determines the parameters of the ellipse to be fitted into the iris boundary. Consider the following example. The iris image in Fig. 12 is partitioned into 5 regions. The regions E1, E3, and E5 contain the boundary between iris and sclera. The other two regions contain boundaries between iris and eyelids and eyelashes. The corresponding unwrapped iris is shown on the right panel in Fig. 12. It is easy to see that the parameters of the ellipse to be fitted in the iris can be found by detecting the edges in the regions E1, E3, and E5.

3) *The Off Center Penalty*: Although the center of the pupil and the center of the iris are known to be non-coaxial, we assume that they are located close to one another. To compensate for this effect we involve an off center penalty term  $\xi(x_{i0}, y_{i0})$  defined as

$$\xi(x_{i0}, y_{i0}) = \frac{1}{1 + \frac{\min(a, b)}{\max(a, b)} \frac{(x_{i0} - x_{p0})^2 + (y_{i0} - y_{p0})^2}{d_{max}^2}},$$

where the maximum off center distance  $d_{max}$  is a predetermined quantity. In our experiment we set it to  $0.4 \times \max(a, b)$ . The penalty term involves ellipse parameters  $a$  and  $b$ , since the distance between pupil center and iris center increases as the off-angle value increases. After substituting  $\xi(x_{i0}, y_{i0})$  into (4), the

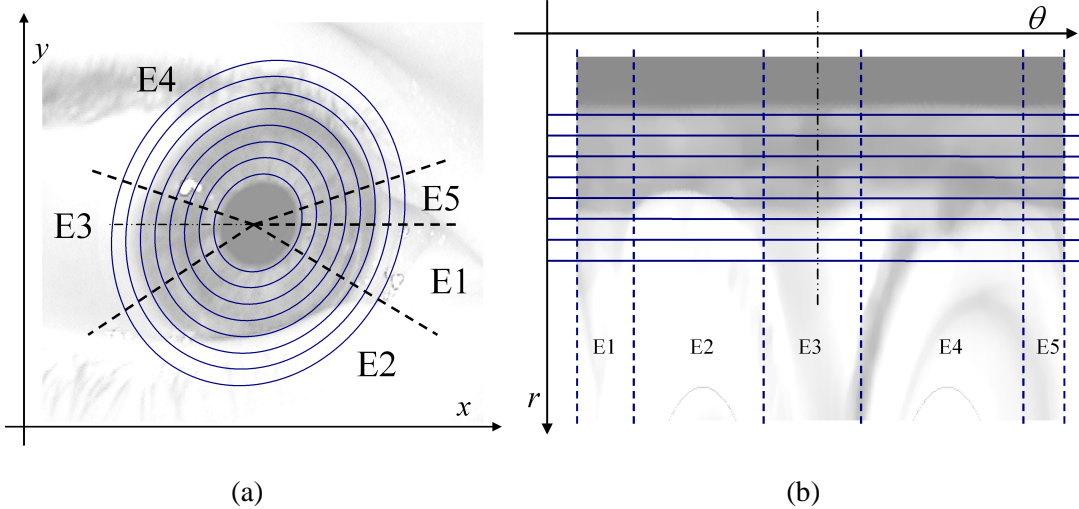


Fig. 12. (a) The original image showing an off-angle iris and (b) the same iris transformed into the circular coordinate system and unwrapped. The regions E1, E3, and E5 contain the true boundary between the iris and sclera and are used to find the parameters of the ellipse to be fitted into the iris.

equation (4) becomes:

$$\max_{r,(x_{i0},y_{i0})} \left[ \xi(x_{i0},y_{i0}) \frac{1}{L(r, x_{i0}, y_{i0})} \oint_{B(r, x_{i0}, y_{i0})} F(\nabla(I(x, y))) ds \right]. \quad (7)$$

Fig. 13 demonstrates the relationship between the off center distance and the off angle value using an error bar plot. We used the WVU Off-angle dataset. Note that off center penalty is smaller for off-angle cases compared with frontal view cases because of the scale factor  $\frac{\min(a,b)}{\max(a,b)}$ .

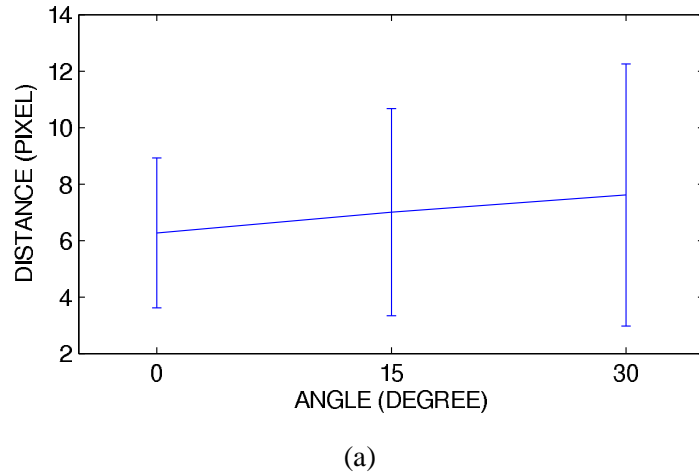


Fig. 13. The relationship between the off center distance in pixels and the off angle in degrees

4) *Contrast Compensation*: Besides heavy occlusion, the uneven illumination of the iris may cause an “offset” during the estimation of the iris boundary, since all points on the boundary are treated equally. An example of the iris is shown in Fig. 14, where the gradient difference along the iris boundary, resulting from an uneven illumination, caused the left edge of the iris to be more pronounced compared to the right edge. This problem can be easily solved by normalizing the gradients before fitting an ellipse. Note that at this stage, the pupil is segmented. Therefore, the iris images can be unwrapped with respect to the pupil center. The right and left portions of the unwrapped iris are then considered separately. The iris boundaries are detected separately too. The summation of the gradient values along the boundary on each side is used to calculate the weights to balance the segmentation. To achieve the correct segmentation of the iris we scale the right and left boundaries of the iris by estimated weights that balance the contribution of the boundaries into the complete ellipse fitted into the iris. The details of the contrast balancing procedure are illustrated in Fig. 15.

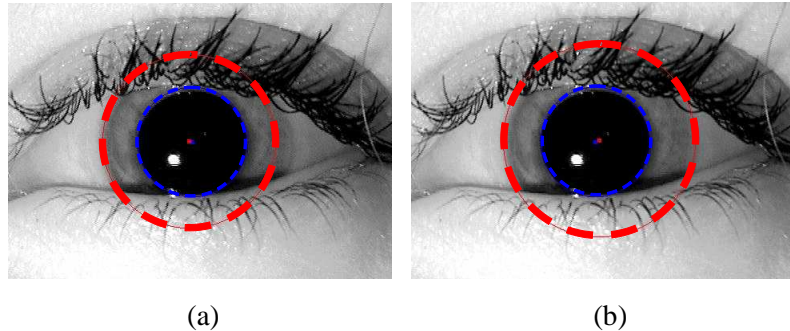


Fig. 14. The result of segmentation (a) before contrast balancing and (b) after application of contrast balancing.

#### D. Occlusion Estimation

The variability of the eyelashes, not only in terms of their position, but also in terms of the direction and intensity, makes occlusion estimation difficult. In this work we implement an occlusion estimation method based on edge detection. This method may not work well on heavily blurred eyelashes and eyelids. For eyelashes, it also can not ensure that all eyelashes are included in the occlusion mask.

Prior to estimating occlusions we apply an adaptive illumination compensation technique. Most of unclear edges due to eyelids are caused by an uneven illumination. An illumination compensation procedure results in brightening shadowed areas and increasing the overall contrast along edges [35]. We involve a Quotient Image-based method [36], [37] to achieve invariance to illumination.

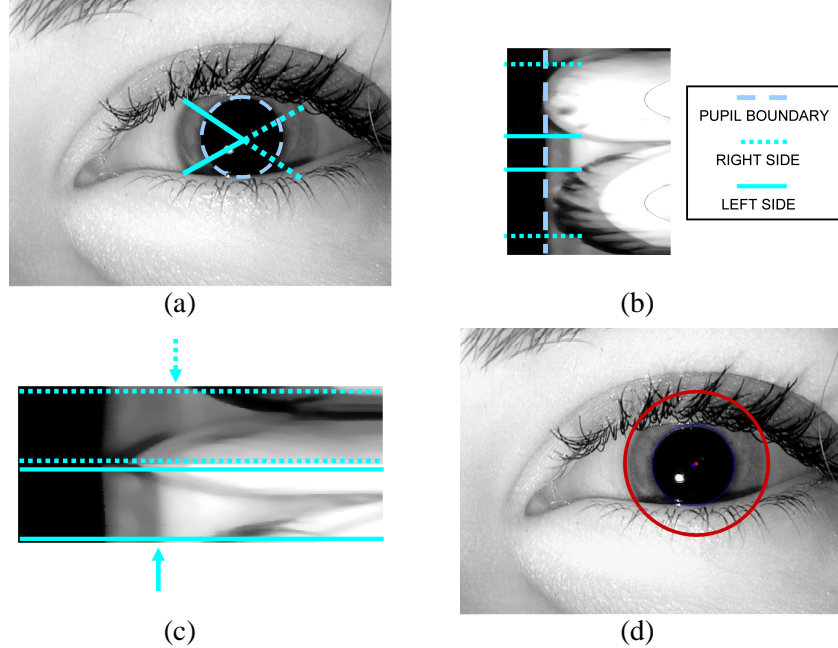


Fig. 15. Contrast balancing procedure: (a) the original image with results of pupil segmentation imposed onto the image, (b) the unwrapped image, (c) the iris boundaries are detected separately for left and right portions of the iris, (d) the result of the final iris detection with different contrast compensation weights added on the both sides.

The process of estimating occlusions is further illustrated in Fig. 16. The main steps include: detection of horizontal edges (Fig. 16-b), smearing of detected edges (Fig. 16-c), selection of the iris area based on the earlier obtained segmentation result (Fig. 16-d and 16-e) and refinement of the estimated mask based on the connectivity information (Fig. 16-f).

To detect horizontal edges, we implement a few steps. We first convolve a horizontal Sobel mask with the iris image. Let  $b_y$  be the result of the convolution. We further compare  $b_y^2$  with the square of the sensitivity threshold  $\lambda$  at every pixel location  $(n_1, n_2)$ . If  $b_y(n_1, n_2)^2 > \lambda^2$  and if it is a local maximum, then a horizontal edge point is detected at position  $(n_1, n_2)$ . The parameter  $\lambda$  has to be adjusted for different datasets. The smaller the value of  $\lambda$ , the higher sensitivity of the algorithm to low contrast edges.

Fig. 17 illustrates two cases. In the first case, the occlusion mask is estimated without application of illumination compensation technique. The second case presents the results of occlusion estimation after illumination invariance is achieved.

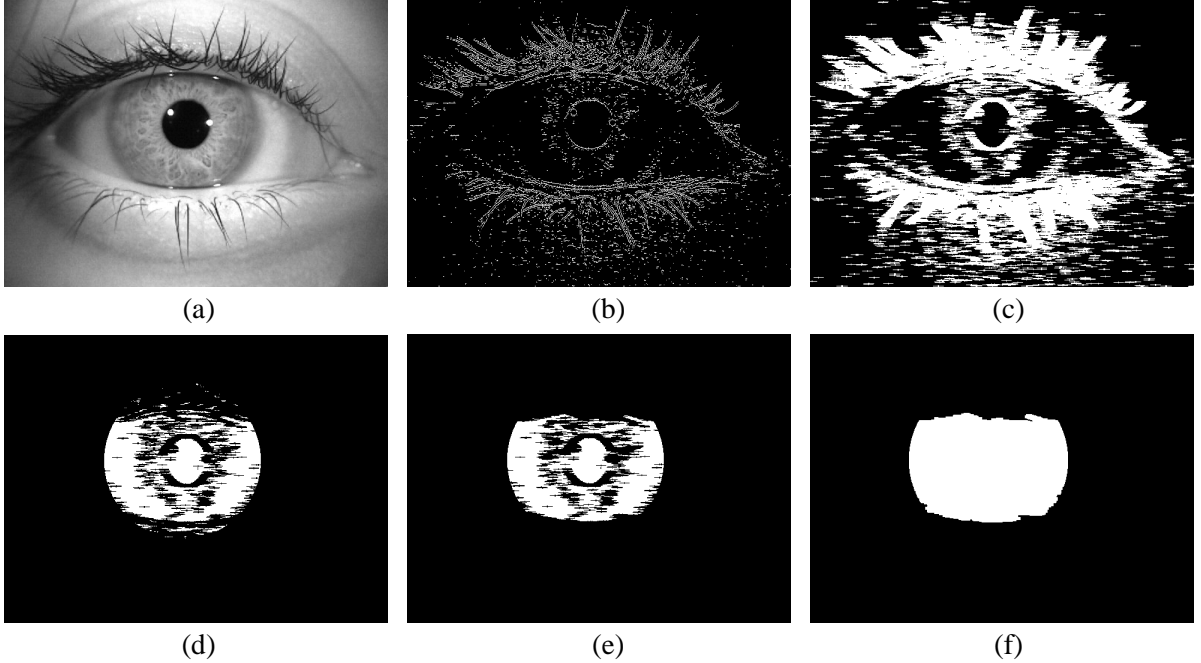


Fig. 16. The evolution of the occlusion mask: (a) the original image, (b) the result of the initial edge detection, (c) the edge information after smearing, (d) the result of combination of the mask and the outcome of iris segmentation, (e) the area selected based on connectivity information, and (f) the final result.

### E. Unwrapping

To unwrap the iris, we involve a technique similar to Camus and Wildes's technique [38]. Both iris and pupil are described by ellipses. The boundaries are sampled and mapped into circles as described in Section II-C.2. The ellipse describing the pupil boundary is given by

$$\begin{cases} x_p(\theta) = a_p \cos(\theta - \phi'_p) \cos \phi_p \\ \quad -b_p \sin(\theta - \phi'_p) \sin \phi_p + x_{p0} \\ y_p(\theta) = a_p \cos(\theta - \phi'_p) \sin \phi_p \\ \quad +b_p \sin(\theta - \phi'_p) \cos \phi_p + y_{p0} \end{cases}, \quad (8)$$

where  $(x_{p0}, y_{p0}, a_p, b_p, \phi_p)$  are the parameters of the ellipse. The iris boundary is described by the ellipse with the parameters  $\{x_{i0}, y_{i0}, a_i, b_i, \phi_i\}$  :

$$\begin{cases} x_i(\theta) = a_i \cos(\theta - \phi'_i) \cos \phi_i \\ \quad -b_i \sin(\theta - \phi'_i) \sin \phi_i + x_{i0} \\ y_i(\theta) = a_i \cos(\theta - \phi'_i) \sin \phi_i \\ \quad +b_i \sin(\theta - \phi'_i) \cos \phi_i + y_{i0} \end{cases}. \quad (9)$$

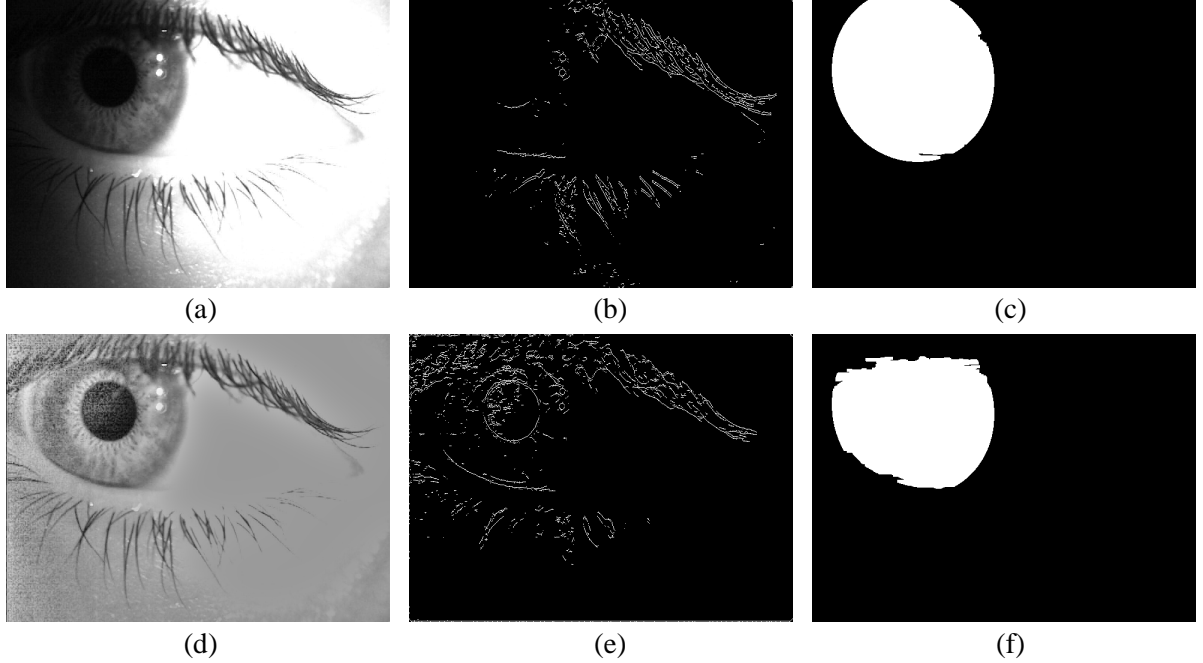


Fig. 17. The evolution of the occlusion mask: (a) the original image, (b) the result of the initial edge detection, (c) occlusion mask obtained without illumination preprocessing, (d) image after illumination compensation, (e) the result of horizontal edge detector, (f) occlusion mask obtained after application of illumination compensation.

The mapping of the point  $(x', y')$  into  $(\theta, r)$ -point in the pseudo-polar coordinate system is described by:

$$\begin{cases} x'(\theta, r) = (1 - r)x_p(\theta) + rx_i(\theta) \\ y'(\theta, r) = (1 - r)y_p(\theta) + ry_i(\theta) \end{cases}, \quad (10)$$

where  $0 < r \leq 1$ ,  $(x_p, y_p)$  is a sample point on the pupil boundary, and  $(x_i, y_i)$  is a sample point on the iris boundary. Finally, the pixel intensity is interpolated using a cubic interpolation method to generate the unwrapped iris.

### III. PERFORMANCE EVALUATION

To verify the performance of the proposed segmentation algorithm, we involve (a) visual (subjective) evaluation and (b) evaluate the influence of the quality of segmentation on recognition performance. The segmentation algorithm is applied to near-IR imagery from a number of public databases. The performance of the algorithm is compared with the performance of two other segmentation algorithms.

#### A. Quality of segmentation: Visual Evaluation

Since the ground truth is not available, we appeal to a subjective (visual) evaluation as shown in Fig. 18. We select two criteria as a measure of visual evaluation: the maximum offset of the pupil boundary,

$\epsilon_p$ , and the maximum offset of the iris boundary  $\epsilon_i$ . The two offsets will be compared with the minimum distance between the iris boundary and pupil,  $min_d$ . All segmentation results will be placed in four

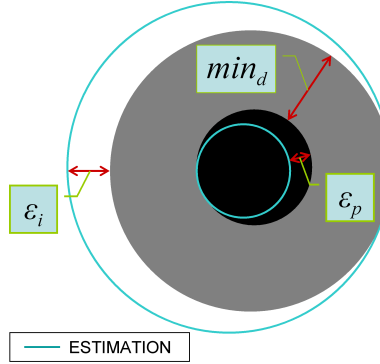


Fig. 18. Criteria used for visual evaluation of the proposed segmentation algorithm.

categories:

**Good:**  $\epsilon_p/min_d < 5\%$  and  $\epsilon_i/min_d < 10\%$ . There is no clear boundary offset between segmentation curves and true iris or pupil boundary. The error of the occlusion estimation is less than 12.5% of unmasked area.

**Fair:**  $(5\% \leq \epsilon_p/min_d < 10\% \text{ and } \epsilon_i/min_d < 20\%)$  or  $(\epsilon_p/min_d < 10\% \text{ and } 10\% \leq \epsilon_i/min_d < 20\%)$ . The error of the occlusion estimation is less than 25% of unmasked area.

**Poor:**  $(10\% \leq \epsilon_p/min_d < 20\% \text{ and } \epsilon_i/min_d < 35\%)$  or  $(\epsilon_p/min_d < 20\% \text{ and } 20\% \leq \epsilon_i/min_d < 35\%)$ . The error of the occlusion estimation is larger than 25% of unmasked area.

**Bad:** Everything else.

Examples of good, fair, poor, and bad segmentation are shown in Fig. 19. Fig. 20 displays two examples of correctly segmented iris images from WVU and WVU-OA datasets.

### B. Segmentation Performance

To analyze the robustness of the proposed segmentation algorithm we evaluate four datasets: CASIA III INT (INT stands for interval), ICE, WVU, and WVU Off-Angle. The WVU data consists of 2453 images, representing 359 different classes captured by an OKI-IrisPass hand-held device at a resolution of  $640 \times 480$ . The number of acquisitions per eye ranged from 2 to 17. This dataset has been verified as non-ideal [2], [4], consisting of predominantly heavy occlusion and strong illumination variation. The WVU Off-Angle (WVU-OA) data consists of 560 images, representing 140 different classes captured at a resolution of  $720 \times 576$ . Each class has 2 frontal images, 1 image at  $15^\circ$ , and 1 image at  $30^\circ$ .

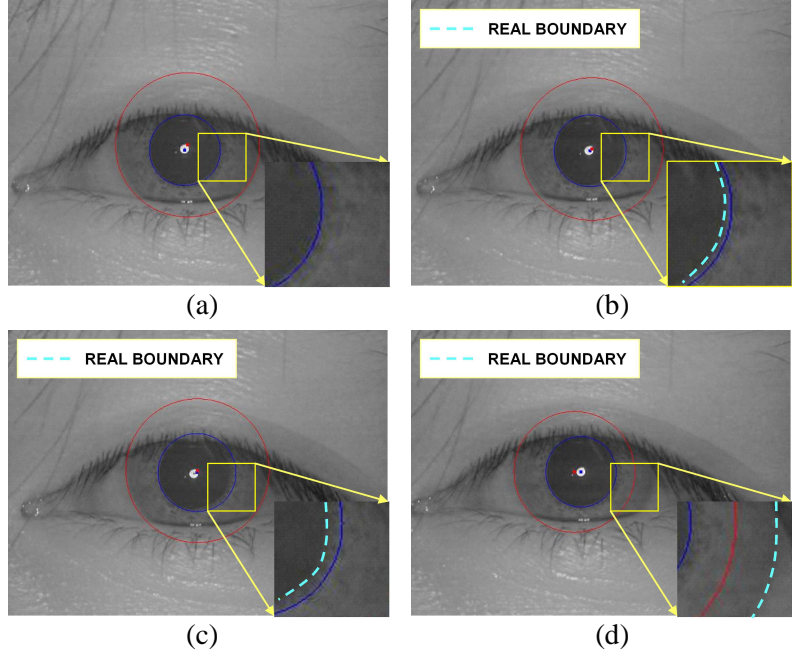


Fig. 19. Examples of: (a) good, (b) fair, (c) poor, and (d) bad segmentations.

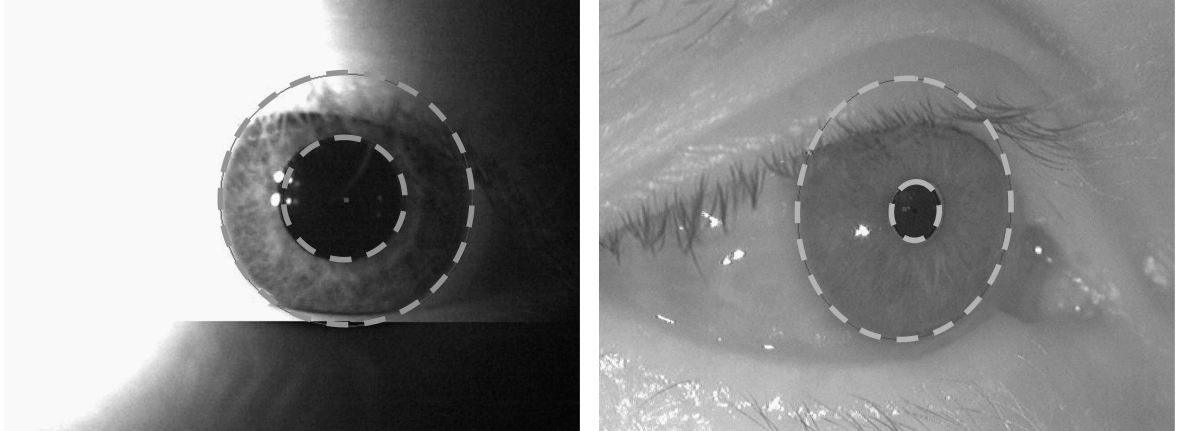


Fig. 20. Examples of correctly segmented iris images from WVU and WVU-OA datasets.

Segmentation performance is evaluated by visual inspection of each image. Segmentation results are classified as either correct (good, fair) or incorrect (poor, bad).

*1) Parameters:* Iris databases used in our experiments have distinct resolution, optical characteristics, and noise. Based on our observation, iris images from ICE dataset have relatively uniform intensity values in the area of pupil excluding the regions of specular reflections. The boundaries between the regions of specular reflection and the pupil are relatively clear except a few cases of heavily blurred images. Iris images from WVU dataset have a larger variance of the pixel intensities within the pupil area and a

large number of images characterized by low contrast. Iris images from WVU-OA dataset are generally of good quality. CASIA III “interval” directory is characterized by complex specular reflections. Based on analyzed characteristics of images from different datasets, we identified a number of parameters of the segmentation algorithm that need to be adjusted for improved segmentation. The main parameters include:

- Maximum pupil intensity value  $\tau$  (introduced in section II-A.1). This is the maximum value of pupil intensity around the area affected by specular reflections.
- A threshold  $\gamma_1$  (introduced in section II-A.1). This is a threshold used to detect regions of specular reflections within the area of pupil.
- A threshold  $\gamma_2$  (introduced in section II-A.1). This is a threshold used to detect specularities in the area outside the pupil.
- A parameter  $\lambda$  used to modify sensitivity of the horizontal edge detector (introduced in section II-D). This parameter is used in the process of occlusion estimation. The parameter is adjusted based on the average image contrast of a dataset.

Table I summarizes the estimated parameters  $\tau$ ,  $\gamma_1$ ,  $\gamma_2$ , and  $\lambda$  for the imagery from four databases.

TABLE I  
PARAMETER SETTINGS FOR DIFFERENT DATASETS

	$\tau$	$\gamma_1$	$\gamma_2$	$\lambda$
CASIA III INT	100	100	240	4
ICE	50	50	240	4
WVU	50	50	240	4
WVU-OA	50	50	240	2.3

2) *Performance Comparison:* We compare our segmentation method against two well established algorithms, Libor Masek’s [39],[40] and Camus and Wildes’s [38] algorithms. Masek’s algorithm is publicly available and its modified C++ version was used as a baseline for the ICE phase I (ICE 2005) competition. We use our own implementation of Camus and Wildes’s algorithm described in [38]. Table II compares the success rate in segmentation of the three algorithms. Overall, the proposed algorithm significantly outperforms the other algorithms. Other algorithms have some natural limitations, such as circle fitting for Masek’s implementation which does not perform well on off-angle images. However, a few cases can be found when the algorithms used for performance comparison outperform our algorithm.

Fig. 21 presents an example, where a simple edge-based circle fitting produces better results than our algorithm. This is an example of heavily occluded iris region.

TABLE II  
SUCCESS RATE IN SEGMENTATION

	Masek	Camus and Wildes	Proposed
CASIA III INT	88.89%	92.39%	99.06 %
ICE	91.20 %	90.79 %	98.95%
WVU	64.77 %	85.24 %	97.92 %
WVU-OA	71.43 %	70.00 %	99.82%

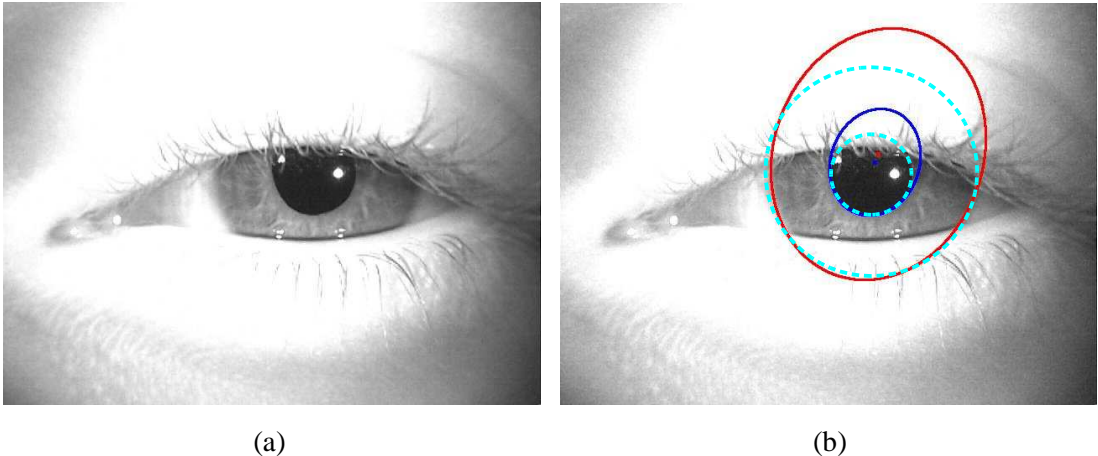


Fig. 21. Segmentation of occluded iris images: (a) the original image (from WVU dataset), (b) circular fit due to a simple edge-based approach (dashed line) and elliptical fit due to our algorithm (solid line).

Table III contains the results of manual evaluation of the segmentation performance of the proposed algorithm. Note that combined “good” and “fair” results provide us with the percentage of correctly segmented iris images.

### C. Recognition Performance

Fig. 22 illustrates ROC performance of our segmentation algorithm compared with the baseline algorithm used in the ICE 2005 competition. Both algorithms use Libor Masek’s encoding algorithm. The difference is in segmentation. The baseline algorithm is described in [39],[40]. The performance of other ICE 2005 participants is not shown, since we do not analyze performance of encoding techniques. For the

TABLE III  
THE RESULTS OF MANUAL PERFORMANCE EVALUATION

Dataset	Correct=Good+Fair	Good	Fair	Poor	Bad	Incorrect=Poor+Bad
CASIA III INT	99.06%	96.31%	2.75%	0.49%	0.45%	0.94 %
ICE	98.95%	91.80%	7.15%	0.17%	0.88%	1.05%
WVU	97.92%	90.05%	7.87%	0.86%	1.22%	2.08%
WVU-OA	99.82%	93.39%	6.43%	0.18%	0%	0.18%

right eye test, our algorithm achieves 97.95% verification rate (VR) at 0.1% false accept rate (FAR), while the baseline algorithms achieves 85.5%. For the left eye test, our algorithm achieves 96.85% VR at 0.1% FAR, while the baseline algorithms achieves 85.45%. Note the substantial improvement in recognition performance due to application of our segmentation algorithm adapted to deal with nonideal iris imagery.

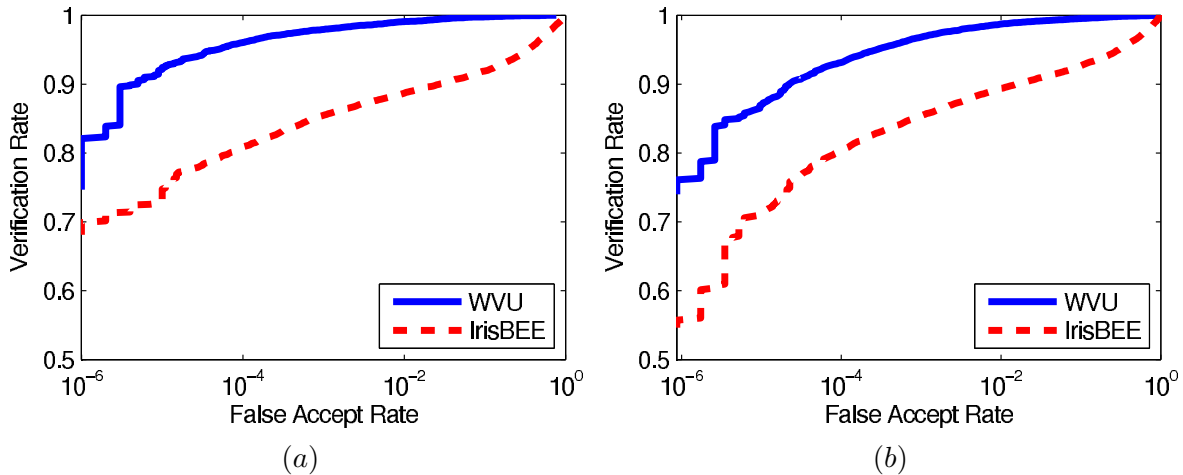


Fig. 22. ROC performance of (a) right and (b) left eye for ICE data. IrisBEE is a version of Masek's algorithm. IrisBEE composed of segmentation, encoding, and matching algorithms was used as a baseline algorithm in ICE 2005. The solid ROC curves on the left and right panels in the figure are obtained using the segmentation algorithm proposed in this paper and encoding and matching algorithms of the IrisBEE.

The speed of the three algorithms was evaluated using a personal computer equipped with Intel® Pentium® IV 3GHz processor and 2GB of RAM. All segmentation techniques were implemented in Matlab. Implementation of our method relied on functions from Statistics and Image Processing Toolboxes. Optimization of the proposed segmentation method was not a focus of this work. Therefore, the results are provided for non-optimized version of our method. On the contrary, implementation of Camus and Wildes's algorithm relies on multiresolution approach (we used functions from a multiresolution

Toolbox in Matlab [41] to reproduce Camus and Wildes's algorithm). The running time of the methods and algorithms is summarized in Table IV. Camus and Wildes's algorithm is more efficient when applied to high resolution (large in size) images. The proposed algorithm performs relatively well, especially if we notice that our algorithm is not optimized.

TABLE IV  
COMPLEXITY (RESOLUTION VS. RUNNING TIME (IN SECONDS))

	Masek	Camus and Wildes	Proposed (step size 1)	Proposed (step size 2)	Proposed (step size 3)
$640 \times 480$	439	69	138	108	101
$480 \times 360$	324	42	85	70	67
$320 \times 240$	89	27	34	30	30
$160 \times 120$	18	10	10	9	9

The proposed non-optimized segmentation procedure may appear to be slow when the algorithm operates on high resolution images. This inefficiency is due to filtering operations and is due to using an exhaustive search to select the best candidate for the iris center. In a database such as ICE 2005 database the off-center distance can reach up to 11 pixels. For the search over a circular area this results in about 380 iris center candidates to consider. The distribution of the off-center distances for ICE 2005 can be found in Fig. 23. An example of the image with a large off-center distance is shown in Fig. 24. This procedure can be sped up considerably by involving multi-resolution analysis similar to the one adopted by Camus and Wildes.

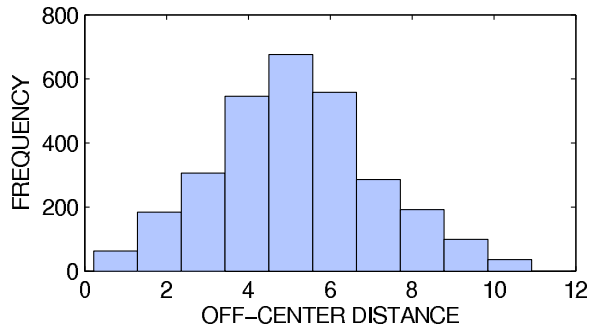


Fig. 23. The distribution of the off-center distances for ICE dataset.

We made the first attempt to speed up our segmentation procedure by applying a hierarchical search algorithm, where prospective centers are sampled roughly at first, then the search is refined. The last three



Fig. 24. An example of large off-center distance image from ICE dataset (243265.tiff).

columns in Table IV are the speed of exhaustive approach and optimized approach due to simply changing the search step to two and three, respectively. The reduction of running time due to the initial optimization is clearly observed. Since our segmentation procedure relies on a large number of enhancement and image processing procedures, changing the search step in searching the iris center may not be sufficient. We believe that applying multi-resolution analysis similar to the one adopted by Camus and Wildes will result in a better solution.

#### IV. CONCLUSIONS AND FUTURE WORK

A methodology for robust iris segmentation designed specifically for non-ideal irises has been proposed. This methodology utilizes shape, intensity, and location information for pupil/iris localization. An ellipse based model is used to contour the estimated boundaries for pupil and iris regions which demonstrates robustness to non-frontal iris images. A contrast balancing technique is introduced to reliably detect iris boundary under the condition of uneven illumination. The occlusion mask is carefully estimated using robust edge detector. We have evaluated four distinct datasets, ideal and non-ideal, in order to demonstrate the robustness of our algorithm. We have compared our results to that of Masek and Camus and Wildes. Using all datasets, we achieve an average increase in segmentation performance of 17.1% over the latter segmentation methodologies. Optimization of the speed of the algorithm was beyond the scope of this paper.

In the future we plan to address a number of problems that we observed while performing this work. We intend to address the issue of the speed of our algorithm. The goal is to make implementation to perform online.

We would also like to explore new methods and processing tools described in the literature on iris segmentation and iris recognition. For example, application of active contours as a tool for a potentially more precise segmentation is a natural extension to our current work. We will use ellipse fitting as an initial guess.

Another direction to take is to design an automatic algorithm evaluating the precision of segmentation (see some preliminary results published in [42]). Since any automatic iris segmentation algorithm faces challenging images that result in poor or bad segmentation, the purpose of an automatic algorithm evaluating the precision of segmentation is to block these images from sending them for further processing and recognition. For example, iris images in Fig. 19 and Fig. 21 present a challenge for our segmentation method.

## V. ACKNOWLEDGEMENTS

The authors would like to thank Nathan D. Kalka for many useful discussions.

## REFERENCES

- [1] H. Proen  a and L. A. Alexandre, "Iris segmentation methodology for non-cooperative recognition," in IEE Proc. - Vision, Image and Signal Processing, Apr 2006, vol. 153, pp. 199-205.
- [2] N. D. Kalka, J. Zuo, N. A. Schmid, and B. Cukic, "Image quality assessment for iris biometric," in Proc. of 2006 SPIE Conf. on Biometric Technology for Human Identification III, Apr 2006, vol. 6202, pp. 62020D-1 - 62020D-11.
- [3] N. D. Kalka, "Image quality assessment for iris biometric," Master's Thesis, The Lane Department of Computer Science and Electrical Engineering. West Virginia University, 2005.
- [4] Y. Chen, S. Dass, and A. Jain, "Localized iris quality using 2-D wavelets," in Proc. of Advances in Biometrics, International Conference ICB'06, 2006, pp. 373-381, Hong Kong, China.
- [5] J. Daugman, "High confidence visual recognition of persons by a test of statistical independence," IEEE Trans. on Pattern Analysis and Machine Intelligence, vol. 15, no. 11, pp. 1148-1161, Nov 1993.
- [6] R. P. Wildes, "Iris recognition: an emerging biometric technology," in Proc. of the IEEE, Sep 1997, vol. 85, pp. 1348-1363.
- [7] X. Liu, K. W. Bowyer, and P. J. Flynn, "Experiments with an improved iris segmentation algorithm," in Proc. of 4th IEEE Workshop on Automatic Identification Advanced Technologies (AutoID), 2005, pp. 118-123.
- [8] Q. Tian, Q. Pan, Y. Cheng, and Q. Gao, "Fast algorithm and application of hough transform in iris segmentation," in Proc. of 3rd Inter. Conf. on Machine Learning and Cybernetics, Shanghai, Aug 2004, vol. 7, pp. 3977-3980.
- [9] C. L. Fancourt, L. Bogoni, K. J. Hanna, Y. Guo, R. P. Wildes, N. Takahashi, and U. Jain, "Iris recognition at a distance.," in Proc. of Inter. Conf. on Audio- and Video-based Biometric Person Authentication AVBPA'05, 2005, pp. 1-13.
- [10] J. De Mira Jr. and J. Mayer, "Image feature extraction for application of biometric identification of iris - a morphological approach," in Proc. of XVI Brazilian Symp. on Computer Graphics and Image Processing (SIBGRAPI'03), Oct 2003, pp. 391-398.
- [11] E. Sung, X. Chen, J. Zhu, and J. Yang, "Towards non-cooperative iris recognition systems," in Proc. of 7th Inter. Conf. on Control, Automation, Robotics and Vision (ICARCV'02), Dec 2002, vol. 2, pp. 990-995.

- [12] J. Zuo, N. K. Ratha, and J. H. Connell, "A new approach for iris segmentation," in IEEE Computer Society Conference on Computer Vision and Pattern Recognition Workshops (CVPR Workshops 2008), Jun 2008, pp. 1–6.
- [13] V. Dorairaj, N. A. Schmid, and G. Fahmy, "Performance evaluation of non-ideal iris based recognition system implementing global ICA encoding," in Proc. of 2005 IEEE Inter. Conf. on Image Processing (ICIP'05), 2005, vol. 3, pp. 285–288.
- [14] A. Abhyankar, L. A. Hornak, and S. Schuckers, "Off-angle iris recognition using bi-orthogonal wavelet network system," in Proc. of 4th IEEE Workshop on Automatic Identification Advanced Technologies (AutoID), Buffalo, NY, Oct 2005.
- [15] J. R. Matey, O. Naroditsky, K. Hanna, R. Kolczynski, D. J. LoIacono, S. Mangru, M. Tinker, T. M. Zappia, and W. Y. Zhao, "Iris on the move: acquisition of images for iris recognition in less constrained environments," in Proc. of the IEEE, Nov 2006, vol. 94, pp. 1936–1947.
- [16] Computer Science Department, Universidade da Beira Interior, "UBIRIS iris database," <http://iris.di.ubi.pt/>.
- [17] N. B. Puhan, N. Sudha, and X. Jiang, "Robust eyeball segmentation in noisy iris images using Fourier spectral density," in 6th International Conference on Information, Communications and Signal Processing, Dec 2007, pp. 1–5.
- [18] S. J. Pundlik, D. L. Woodard, and S. T. Birchfield, "Non-ideal iris segmentation using graph cuts," in IEEE Computer Society Conference on Computer Vision and Pattern Recognition Workshops (CVPR Workshops 2008), Jun 2008, pp. 1–6.
- [19] A. Zaim, M. Quweider, J. Scargle, J. Iglesias, and R. Tang, "A robust and accurate segmentation of iris images using optimal partitioning," in International Conference on Pattern Recognition, Aug 2006, pp. 578–581.
- [20] W. Kong and D. Zhang, "Detecting eyelash and reflection for accurate iris segmentation," International Journal of Pattern Recognition and Artificial Intelligence, vol. 17, no. 6, pp. 1025–1034, 2003.
- [21] X. He and P. Shi, "A novel iris segmentation method for hand-held capture device," in Springer LNCS 3832: International Conference on Biometrics, Jan 2006, pp. 479–485.
- [22] J. Huang, Y. Wang, J. Cui, and T. Tan, "Noise removal and inpainting model for iris image," in International Conference on Image Processing, Oct 2004, pp. 2:869–872.
- [23] J. Daugman, "Probing the uniqueness and randomness of iriscodes: results from 200 billion iris pair comparisons," in Proc. of the IEEE, Nov 2006, vol. 94, pp. 1927–1935.
- [24] J. Daugman, "New methods in iris recognition," in IEEE Transactions on Systems, Man, and Cybernetics, Part B, Sep 2007, vol. 37, pp. 1167–1175.
- [25] G. Shafer, A Mathematical Theory of Evidence, Princeton University Press, Princeton, NJ, 1976.
- [26] Center for Biometric Authentication and Testing, Institute of Automation, Chinese Academy of Sciences, China, "CASIA iris database (ver. 3.0)," <http://www.cbsr.ia.ac.cn/Databases.htm>.
- [27] National Institute of Standards and Technology (NIST), "Iris challenge evaluation," <http://iris.nist.gov/ICE/>.
- [28] S. Crihalmeanu, A. Ross, R. Govindarajan, L. Hornak, and S. Schuckers, "A centralized web-enabled multimodal biometric database," in Proc. of Biometric Consortium Conference 2004 (BCC'2004), Crystal City, VA, USA, Sep 2004.
- [29] Center for Identification Technology Research, "WVU off-angle iris database," <http://www.citer.wvu.edu>.
- [30] T. Chan, J. Shen, and L. Vese, "Variational PDE models in image processing," in Notice of Amer. Math. Soc., Jan 2003, vol. 50, pp. 14–26.
- [31] R. J. Serfling, Approximation Theorems of Mathematical Statistics, Wiley-Interscience, 1980.
- [32] J. S. Lim, Two-Dimensional Signal and Image Processing, Prentice Hall, Englewood Cliffs, NJ, 1990.
- [33] J. Daugman, "How iris recognition works," IEEE Trans. Circuits and Syst. for Video Tech., vol. 14, no. 1, pp. 21–30, Jan 2004.

- [34] P. Burve and X. Li, "Robust preprocessing techniques for nonideal iris recognition," in Proc. of Biometric Consortium Conference 2005 (BCC'2005), Virginia, USA, Sep 2005.
- [35] H. Wang, S. Z. Li, and Y. Wang, "Face recognition under varying lighting conditions using self quotient image," in Proc. of the Sixth IEEE Inter. Conf. on Automatic Face and Gesture Recognition (FGR'04), May 2004, pp. 819– 824.
- [36] A. Shashua and T. Riklin-Raviv, "The quotient image: class-based re-rendering and recognition with varying illuminations," Trans. on Pattern Analysis and Machine Intelligence, vol. 23, no. 2, pp. 129–139, 2001.
- [37] T. Riklin-Raviv and A. Shashua, "The quotient image: class based recognition and synthesis under varying illumination," in Proc. of the 1999 Conf. on Computer Vision and Pattern Recognition, 1999, pp. 566–571.
- [38] T. A. Camus and R. Wildes, "Reliable and fast eye finding in close-up images," in Proc. of 16th Inter. Conf. on Pattern Recognition, Aug 2002, vol. 1, pp. 389–394.
- [39] L. Masek, "Recognition of human iris patterns for biometric identification," Bachelor's Dissertation, The School of Computer Science and Software Engineering, The University of Western Australia, 2003.
- [40] L. Masek and P. Kovesi, "MATLAB source code for a biometric identification system based on iris patterns," Computer Science and Software Engineering, The University of Western Australia, 2003.
- [41] E. P. Simoncelli, "matlabPyrTools," <http://www.cns.nyu.edu/~lcv/software.html>.
- [42] J. Zuo and N. A. Schmid, "An automatic algorithm for evaluating the precision of iris segmentation," in International Conference on Biometrics: Theory, Applications, and Systems (BTAS 2008), Sep 2008.